Perceptual Cycles Travel Across Retinotopic Space

Camille Fakche[1] [iD] and Laura Dugué[1,2] [iD]

Abstract

■ Visual perception waxes and wanes periodically over time at low frequencies (theta: 4–7 Hz; alpha: 8–13 Hz), creating "perceptual cycles." These perceptual cycles can be induced when stimulating the brain with a flickering visual stimulus at the theta or alpha frequency. Here, we took advantage of the well-known organization of the visual system into retinotopic maps (topographic correspondence between visual and cortical spaces) to assess the spatial organization of induced perceptual cycles. Specifically, we tested the hypothesis that they can propagate across the retinotopic space. A disk oscillating in luminance (inducer) at 4, 6, 8, or 10 Hz was presented in the periphery of the visual field to induce perceptual cycles at specific frequencies. EEG recordings verified that the brain responded at the corresponding inducer frequencies and their first harmonics. Perceptual cycles were assessed with a concurrent detection task—target stimuli were displayed at threshold contrast (50% detection) at random times during the inducer. Behavioral results confirmed that perceptual performance was modulated periodically by the inducer at each frequency. We additionally manipulated the distance between the target and the inducer (three possible positions) and showed that the optimal phase, that is, moment of highest target detection, shifted across target distance to the inducer, specifically when its flicker frequency was in the alpha range (8 and 10 Hz). These results demonstrate that induced alpha perceptual cycles travel across the retinotopic space in humans at a propagation speed of 0.3–0.5 m/sec, consistent with the speed of unmyelinated horizontal connections in the visual cortex. ■

INTRODUCTION

Our perception phenomenologically appears continuous over time. Yet, our perceptual performance fluctuates periodically between favorable and less favorable moments (VanRullen, 2016; VanRullen & Koch, 2003). These "perceptual cycles" have been observed in human and nonhuman primates at low frequencies (theta: 4–7 Hz; alpha: 8–13 Hz; Michel, Dugué, & Busch, 2022; Senoussi, Moreland, Busch, & Dugué, 2019; Dugué & VanRullen, 2017; Dugué, Marque, & VanRullen, 2015; Huang, Chen, & Luo, 2015; Song, Meng, Chen, Zhou, & Luo, 2014; Fiebelkorn, Saalmann, & Kastner, 2013; Landau & Fries, 2012; VanRullen, 2007; VanRullen, Reddy, & Koch, 2005, 2006; Purves, Paydarfar, & Andrews, 1996; for reviews, see Re, Karvat, & Landau, 2023; Kienitz et al., 2022) and can be induced by flickering visual stimuli (Kizuk & Mathewson, 2017; Ten Oever & Sack, 2015; Henry, Herrmann, & Obleser, 2014; Spaak, de Lange, & Jensen, 2014; De Graaf et al., 2013; Henry & Obleser, 2012; Mathewson et al., 2012; Stefanics et al., 2010). Electrophysiological recordings showed that perceptual cycles correlate with brain oscillations, and specifically their phase, at the same frequencies (Fakche, VanRullen, Marque, & Dugué, 2022; Samaha, Gosseries, & Postle, 2017; Fiebelkorn, Snyder, et al., 2013; Hanslmayr, Volberg,

Wimber, Dalal, & Greenlee, 2013; Dugué, Marque, & VanRullen, 2011; Busch & VanRullen, 2010; Busch, Dubois, & VanRullen, 2009; Mathewson, Gratton, Fabiani, Beck, & Ro, 2009; Valera, Toro, John, & Schwartz, 1981). Yet, this phase effect accounts for less than 20% of the trial-by-trial variability in perceptual performance (Fakche et al., 2022; Samaha et al., 2017; Baumgarten, Schnitzler, & Lange, 2015; Dugué et al., 2011, 2015; Busch & VanRullen, 2010; Busch et al., 2009). Here, we build upon the well-known organization of the visual system and propose to fill this gap by assessing the spatial organization of induced perceptual cycles.

Visual input is topographically decomposed in the visual cortex; that is, there is a topographic correspondence between the visual space and the cortical space called retinotopy (for a review, see Wandell & Winawer, 2011). Neural populations in the retinotopic cortex are connected by intracortical networks of long-range unmyelinated horizontal axons of up to several millimeters (for a review, see Chavane, Perrinet, & Rankin, 2022). Interestingly, invasive recordings in animals showed that brain activity originating from a specific location in the retinotopic cortex can propagate across the map (e.g., Davis, Muller, Martinez-Trujillo, Sejnowski, & Reynolds, 2020; Chemla et al., 2019; Townsend et al., 2015; Yang, Heeger, Blake, & Seidemann, 2015; Zanos, Mineault, Nasiotis, Guitton, & Pack, 2015; Muller, Reynaud, Chavane, & Destexhe, 2014; Zhang et al., 2012; Benucci, Frazor, & Carandini, 2007; Jancke, Chavane, Naaman, & Grinvald,

[1]Université Paris Cité, CNRS, Integrative Neuroscience and Cognition Center, Paris, France, [2]Institut Universitaire de France

2004; Bringuier, Chavane, Glaeser, & Frégnac, 1999). Here, we test the hypothesis that induced perceptual cycles can propagate across the retinotopic visual space presumably because of horizontal connections in the retinotopic visual cortex.

Sokoliuk and VanRullen (2016) showed in a psychophysics experiment that induced 5- and 10-Hz perceptual cycles assessed by detection of a low-contrast target stimulus propagated across the retinotopic visual space. Specifically, a brief target at threshold contrast was presented at three possible distances from a continuously oscillating disk in the periphery of the visual field (inducer). They showed that the optimal behavioral phase (the moment of the oscillating disk leading to the highest performance in target detection) shifted as a function of distance between target and inducer. Here, we used the same psychophysics approach. We additionally recorded EEG to identify the shape of the induced-brain activity and used eye tracking to ensure successful fixation of the center of the screen, critical for stable retinotopic representation. Other critical changes were made to the design, including the size of the targets, which was adjusted to cortical magnification, so that each stimulus activated the same number of neurons in the retinotopic cortex. In addition, we parametrized the frequencies by testing four different frequencies in the theta/alpha range (4, 6, 8, and 10 Hz), which was done in each participant ($n = 17$) to ensure robust statistical analyses (in Sokoliuk and VanRullen, $n = 5$ for 5 Hz, $n = 7$ for 10 Hz, and $n = 15$ for a 10-Hz replication set). Finally, we added a control experiment to ensure that the results were not because of low-level luminance masking (in Sokoliuk and VanRullen, the control that was used was designed in a way that could have interacted with the attention of the participant).

Our study assessed the propagation of induced perceptual cycles across the retinotopic space. Contrary to the earlier study (Sokoliuk & VanRullen, 2016), our results demonstrate that alpha-induced perceptual cycles, and not theta, traveled across the retinotopic space in human observers at a propagation speed ranging from 0.3 to 0.5 m/sec, consistent with the conduction delay of long-range horizontal connections in the visual cortex (Girard, Hupé, & Bullier, 2001; Nowak & Bullier, 1996; Shao & Burkhalter, 1996).

METHODS

Participants

Eighteen participants (nine women, 16 right-handed; age: mean $\pm$ SD = 26.2 $\pm$ 4.1 years) were recruited for the main experiment. One participant was excluded from the analysis because the number of false alarms exceeded the number of targets presented. Fifteen participants (seven women, 13 right-handed; age: mean $\pm$ SD = 25.5 $\pm$ 3 years) were recruited for the additional Control Experiment 1 (see Control Experiment 1: Flashing Disk section

below); and 15 participants (nine women; age: mean $\pm$ SD = 26.1 $\pm$ 4.3 years), for Control Experiment 2 (see Control Experiment 2: Broadband Oscillating Disk section). The number of participants was decided based on previous studies using flickering visual stimuli to induce perceptual cycles (mean $\pm$ SD number of participants from a sample of representative studies = 15.5 $\pm$ 9.3; Kizuk & Mathewson, 2017 [$n = 42$]; Sokoliuk & VanRullen, 2016 [$n = 7$, $n = 15$, $n = 5$, $n = 4$]; Ten Oever & Sack, 2015 [$n = 20$]; Henry et al., 2014 [$n = 17$]; Spaak et al., 2014 [$n = 19$]; De Graaf et al., 2013 [$n = 21$, $n = 18$]; Henry & Obleser, 2012 [$n = 12$]; Mathewson et al., 2012 [$n = 13$]; Stefanics et al., 2010 [$n = 11$, $n = 13$]). All participants were free from medication affecting the central nervous system, reported no history of psychiatric or neurological disorders, gave their written informed consent, and were compensated for their participation. The study was approved by the local French ethics committee Ouest IV (No. 20.04.16.71057) and followed the Declaration of Helsinki.

Stimuli

Stimuli were designed with Psychtoolbox 3.0.12, running in MATLAB R2014b 64-bit (The MathWorks), and displayed with a PROPixx projector (VPixx Technologies), on a 139 × 77.5 cm projection screen (960 × 540 pixels, 480-Hz refresh rate), at a 122-cm distance. Three different stimuli were generated: a fixation cross, a peripheral disk, and three small dots (targets). The arms of the fixation cross measured 0.15° in length and 0.03° in width. The size and position of the targets were computed according to cortical magnification (human cortical magnification factor $= \frac{23.07}{eccentricity + 0.75}$; Horton & Hoyt, 1991) so that each target (diameter) represented a 0.8-mm portion of the cortex spaced by 0.8 mm edge-to-edge (radius: 0.09°, 0.1°, and 0.12°; eccentricity: 4.1°, 4.5°, and 4.9°). The peripheral disk (inducer) was displayed on the lower right corner at 7.5° of eccentricity (from the center of the disk; radius: 1.75°). The background color was black, and the fixation cross was at 50% of contrast relative to the background. Target contrasts were titrated for each participant, each position, and each frequency, using a staircase procedure (see below). The peripheral disk was oscillating sinusoidally in luminance, from black to white (i.e., from 0% to 100% of contrast; one period: black to white to black), at frequencies in the theta and alpha range of 4.07, 6.13, 8.27, and 10.43 Hz. For clarity, we rounded these values to 4, 6, 8, and 10 Hz.

Eye Tracker

For each participant, the head was maintained with a headrest and chin rest. An infrared video-camera system (EyeLink 1000 Plus 5.08, SR Research) was used to ensure that participants maintained their gaze on the fixation

cross throughout the block. The block only started when participants were successfully maintaining fixation. When a gaze deviation of $>2°$ from the center of the screen was detected during the presentation of a target (-150 to $+100$ msec around target onset) or a blink, we considered that the participant broke fixation, and the trial was removed from the analysis (mean $\pm$ SD = 129.1 $\pm$ 120.9 trials on average across participants, leading to a total number of trials $\pm$ SD of 5015.2 $\pm$ 199.9 per participant, for the main experiment). Supernumerary blocks were added at the end of each run to compensate for rejected trials. Participants received feedback at the end of each block to remind them to minimize blinking and to maintain fixation.

EEG

EEG was recorded using a 64-channel actiCHamp system (Brain Products GmbH). The ground was placed at the FPz position, and the right mastoid was used as reference (DC recording; 1000-Hz sampling rate).

Experimental Design

Participants performed five sessions: four psychophysics sessions (one session for each induced frequency; frequency order randomized across participants) and one EEG session. The psychophysics sessions were composed of the staircases and two runs of 50 blocks each. The EEG session contained four runs of 24 blocks each (one run for each induced frequency).

For both the staircases and the main task, each block lasted 30 sec during which the peripheral disk continuously oscillated in luminance. Six to 18 targets were presented at random times (excluding the first and last seconds and with at least a 1-sec interval between targets) during three frames (6.3 msec) according to a decreasing probability distribution (~10 targets per block on average). The number of targets for the three positions was randomized across blocks (and pseudorandomized across runs). Participants were instructed to press the space bar when they detected a target (in a 1-sec time window after which their response was not considered; target presentation and response window composed a trial).

A one-up/one-down staircase with decreasing steps was performed separately for each target position to titrate the contrast of the target to reach about 50% detection. Each staircase was composed of seven blocks, as described above, except that the targets appeared always at the same position. During the main task, target contrasts were adjusted every 15 blocks by multiplying the target contrasts to a factor y varying between 0.5 and 1.5 based on the detection performance for each target. y is calculated as follows:

$$y = 1.5 - \frac{1}{1 + e^{-0.05(x-50)}}$$

with x as the detection performance. This procedure maintained detection performance at the same averaged level across the entire session. Target contrasts averaged (mean $\pm$ SEM) across participants were as follows: 3.2 $\pm$ 0.45%, 2.2 $\pm$ 0.27%, and 2.88 $\pm$ 0.38% for Positions 1, 2, and 3, respectively, for the 4 Hz-induced frequency; 3.35 $\pm$ 0.55%, 2.2 $\pm$ 0.29%, and 2.68 $\pm$ 0.27% for Positions 1, 2, and 3, respectively, for 6 Hz; 3.16 $\pm$ 0.31%, 2.1 $\pm$ 0.19%, and 2.55 $\pm$ 0.18%, for Positions 1, 2, and 3, respectively, for 8 Hz; and 3.03 $\pm$ 0.31%, 2.02 $\pm$ 0.17%, and 2.45 $\pm$ 0.16%, for Positions 1, 2, and 3, respectively, for 10 Hz.

EEG Analysis

Analyses were performed with EEGLab 13.6.5 (Delorme & Makeig, 2004; Swartz Center for Computational Neuroscience, UC San Diego, California) running in MATLAB.

Preprocessing

EEG data and channel location were imported into EEGLab. EEG data were rereferenced to the average of the right and left mastoids. A high-pass filter at 0.1 Hz and a notch filter between 48 and 52 Hz were applied, to respectively remove slow drifts and 50-Hz electric noise. The signal was further downsampled to 512 Hz. Visual inspection allowed to identify electrodes with a low signal-to-noise ratio (SNR), which were then interpolated (spherical interpolation). Independent component analysis was performed to remove blink components, after a visual inspection of their time courses and topographies. Data were epoched from trial onset (0 sec) to the end of the block onset (+30 sec).

Fast Fourier Transform

Fast Fourier transform (FFT) was computed (MATLAB function: *fft*) on 30-sec epoched EEG data, and the amplitude was extracted for each electrode, epoch, and frequency. The SNR was computed on the amplitude extracted from the FFT, for each electrode, as the ratio of the amplitude at each frequency to the average of the 20 surroundings frequencies (10 frequencies on either side, excluding the immediately adjacent frequencies; note that the SNR could mathematically not be estimated at the edges of the spectra), as described in Rossion, Prieto, Boremanse, Kuefner, and Van Belle (2012) and Liu-Shuang, Norcia, and Rossion (2014). SNR averaged across participants, epochs, and electrodes was plotted to ensure that the oscillating disk successfully induced brain activity at the corresponding frequency. Note that an SNR > 1 indicates that there is a difference between the amplitude of the EEG signal at a given frequency and its neighboring ones. Topographies were plotted at the peak of the induced frequency and its first harmonic.

ERPs

Previously preprocessed EEG time series were further bandpass filtered between 1.5 and 30 Hz and baseline corrected from −400 to 0 msec from block onset. Epochs of 1 sec were defined (time-locked to a full-black disk), excluding the first second of each 30-sec block to avoid the transient EEG response because of stimulus onset. Participants' ERPs were computed as the averaged of all resulting epochs. ERPs averaged across participants for electrode Oz were plotted with the *SEM*. Electrode Oz was selected because it is the electrode with the highest amplitude across the four induced frequencies. The ERP plots allowed us to identify that the induced brain activity was composed of two sinusoidal brain signals, one at the induced frequency and the second at its first harmonic. Therefore, a complex sine function was fitted to the behavioral data.

FFT on ERPs

FFT was computed (1500 points of zero padding) on the 1-sec Oz ERP for each participant. The amplitude was extracted, and the SNR was computed as previously described.

Behavioral Analysis

Behavioral analyses were performed with MATLAB R2014b (The MathWorks). The following dependent variables were computed: hit rates as the main dependent variable, that is, percentage of correct responses, and median RTs as secondary dependent variables, for each target position and frequency. Hit rates averaged across frequencies were as follows: 47.65 ± 0.85% (mean ± *SEM*), 46.12 ± 0.81%, and 45.02 ± 0.79% for Positions 1, 2, and 3, respectively. Median RTs averaged across frequencies were 512 ± 7 msec (mean ± *SEM*), 512 ± 7 msec, and 512 ± 8 msec for Positions 1, 2, and 3, respectively. A two-way repeated-measures ANOVA was performed for each dependent variable to assess the effect of Frequency and Target Position. For hit rates, there was a main effect of Target Position, $F_{(2, 32)} = 11.46$, Sum of Squares (SS) = 236.74, $p < .01$, $\eta^2 = 41.75$, but no effect of Frequency, $F_{(3, 48)} = 1.58$, SS = 76.31, $p = .2$, $\eta^2 = 8.99$, nor of their interaction, $F_{(6, 96)} = 0.36$, SS = 12.66, $p = .9$. For median RTs, there was no main effect of Frequency, $F_{(3, 48)} = 2.08$, SS = 4093.43, $p = .11$, $\eta^2 = 11.55$, nor a main effect of Target Position, $F_{(2, 32)} = 0.04$, SS = 12.38, $p = .96$, $\eta^2 = 0.25$, nor of their interaction, $F_{(6, 96)} = 1.02$, SS = 622.66, $p = .41$. The absence of a significant interaction between frequency and target positions in any of these two tests confirms successful contrast manipulation; that is, changes in detection performance across target positions are not different across frequencies (in the absence of such interaction, main effects will not be

further interpreted; importantly, the optimal phase can be properly estimated as performance did not reach ceiling or floor for any of the conditions, which was the purpose of the staircase procedure). As argued in Kienitz, Schmid, and Dugué (2022) and VanRullen and Dubois (2011), RT fluctuations do not unambiguously demonstrate rhythms in cognitive processes as they can also be the by-product of the external stimulation and are sensitive to changes in decision criteria (Dugué, Merriam, Heeger, & Carrasco, 2018, 2020; Carrasco & McElree, 2001; Wickelgren, 1977; Reed, 1973). The behavioral phase analyses thus focused on hit rates as the main dependent variable.

Phase Effect on Detection Performance

Each target was assigned to one of seven phase bins of the periodic stimulation depending on the delay at which they appeared during the block. There were 124 blocks with, on average, 10 targets per block for each frequency, that is, ~1240 trials per frequency in total, resulting in ~413 trials per position and ~60 trials per phase bin. Hit and false alarm rates were computed for each target position, frequency, and phase bin. For each block and target position, false alarms (participants reported perceiving a target while no target had been presented; participants were instructed to respond in the 1-sec window after the target, after which the response was considered a false alarm) were binned as a function of the phase of the oscillating disk; that is, the phase of the false alarms depended on the phase bin of the participant's response. To allow for a fair comparison between hit and false alarms, only the false alarms that were in the same phase bins as the targets (but in a different 100-msec period) were considered for further analysis (e.g., if two targets were presented at Position 1 within the given block, and binned in Bins 2 and 6, only false alarms that were binned in Bins 2 and 6 were considered for further analysis). To allocate a false alarm to one of the three target positions (a false alarm is, by definition, at none of the position), a bootstrap procedure was performed (100 repetitions).

Given the ERP results (see Figure 2) showing a complex neural response composed of the induced frequency and its first harmonic, a complex sine function was fitted to behavioral data (Equation 1) with the following free parameters: $x[1]$ and $x[2]$ as the amplitude and the phase offset of the induced frequency, respectively; $x[3]$ and $x[4]$ as the amplitude and the phase offset of the first harmonic, respectively; and $x[5]$ as the baseline level. Note that, because we did not have a priori hypothesis regarding the shape of the induced behavioral response, we selected the shape of the closest proxy, that is, the evoked response. To find the parameters that best fit the data, we used a least squares cost function, that is, the cost function computed the total squared errors, that is, the sum of squared errors, between the fit and the data, thus giving

a measure of how well the data are fitted. The best fit is the one whose parameters minimize the total error (Watt, Borhani, & Katsaggelos, 2020).

$$x[1] \times (\sin(2 \times \pi \times T + x[2])) + x[3]$$
$$\times \left(\sin \left(2 \times \pi \times \frac{T}{2} + x[4] \right) \right) + x[5] \qquad (1)$$

We then performed a Monte Carlo procedure on the fitted amplitude (see Statistical Analyses section) to evaluate whether the fitted data were modulated periodically as a function of the phase. Note that false alarms were low in each phase bin (<0.5%) and not significantly modulated periodically after Bonferroni correction across frequencies and positions (p value threshold < .004, corresponding to a z score threshold of 2.64 and a Cohen's d threshold of 1.66). Consequently, in the next steps of the analysis, only hit rates were considered.

A group-level analysis was also performed. Empirical and surrogate data were averaged across participants, and the same Monte Carlo procedure was performed.

Variance Explained by the Spatial Organization of Targets

We hypothesized that taking into consideration the spatial organization of induced perceptual cycles should explain more variance in the behavioral phase effect; that is, the difference of performance between the optimal and nonoptimal behavioral phases should be larger when considering the spatial location of the target rather than disregarding where the target appears relative to the luminance disk. To test this hypothesis, we compared the amplitude modulation (difference in hit rate between the optimal and nonoptimal behavioral phases) averaged across the three target positions with the amplitude modulation computed across targets independently of their position, for each frequency separately. Specifically, hit rates were computed for each participant, frequency, and phase bin, regardless of target position. We used a subsampling procedure (1000 repetitions) to equalize the number of trials (pooled across all three target positions) to the number of trials for each position. Two-tailed t tests were used to assess whether the amplitude modulation averaged across the three target positions was significantly different from the amplitude modulation computed across targets independently of their position, for each frequency.

Behavioral Optimal Phase Shift Between Target Positions

The optimal phase, that is, the position on the fitted curve at maximal performance, was extracted for each target position and frequency, on data averaged across participants and for each participant individually. We asked whether the optimal phase shift as a function of target

positions was different between the four induced frequency conditions, that is, whether there is a significant interaction between frequency and target position.

The optimal phases were converted in radians. A one-cycle sine wave was generated with the phase offset of the oscillating disk, and phase values were extracted in radians along the entire cycle. The optimal phase extracted from data fitting was then calculated in radian based on this one-cycle sine wave fit participant-by-participant. We then obtained rose plots of all individual optimal phases with the function *circ_plot* from the Circular Statistics Toolbox (see Figure 4; Berens, 2009, www.jstatsoft.org/v31/i10), for each frequency and target position. A Harrison–Kanji test was performed (a two-way ANOVA for circular data; *circ_hktest* from the Circular Statistics Toolbox) on the individual optimal phases, with frequency and position as factors. An interaction would indicate that the effect of position on the optimal phase differs across frequency conditions. We further computed the pairwise phase difference with the function *circ_dist* participant-by-participant, for each pair of positions (Positions 1 and 2, Positions 1 and 3, and Positions 2 and 3), and we tested whether the pairwise phase difference was significantly different against 0, that is, null difference, for each frequency and pair of positions, with a Watson–Williams test (function *circ_wwtest*) from the Circular Statistics Toolbox. p Values were Bonferroni corrected for multiple comparisons across target positions and frequencies (p value threshold < .004, corresponding to a z score threshold of 2.64 and a Cohen's d threshold of 1.66).

Control Experiment 1: Flashing Disk

This control experiment was designed based on Sokoliuk and VanRullen (2016).

Experimental Design

The targets were of the same size and location as in the main experiment. The peripheral disk was, however, not modulated sinusoidally but was flashed (during three frames, for 6.3 msec) at seven different levels of luminance (seven contrast levels: 5%, 20.8%, 36.7%, 52.5%, 68.3%, 84.2%, and 100%) at the same time as target onset to test for luminance masking. There was 20% of catch trials in which the disk was flashed, but not the target.

As for the main experiment, the control experiment first included a staircase procedure to adjust the contrast of each target, for each participant, to reach 50% detection. In seven blocks, the luminance of the disk was set at 50% contrast. For each block, 6–18 targets were presented (~10 targets/trials per block on average); thus, the staircase procedure contained an average of 70 trials.

Then, participants performed four runs of 38 blocks each in two separate experimental sessions of approximately 1 hr 30 min each (no EEG recording for this control

experiment). Each contrast level was displayed the same number of times (~217 targets per contrast level). Target contrasts were adjusted every 15 blocks to maintain the same detection level across the entire session.

Analyses

Hit rates, that is, percentage of correct detection, median RTs, and target contrasts were computed for each target position. Hit rates were $57.18 \pm 1.1\%$ (mean $\pm$ *SD*), $51.74 \pm 0.35\%$, and $45.82 \pm 0.76\%$ for Positions 1, 2, and 3, respectively. Median RTs were 474 ± 2 msec (mean $\pm$ *SD*), 511 ± 3 msec, and 525 ± 3 msec for Positions 1, 2, and 3, respectively. Target contrasts were $0.61 \pm 0.01\%$ (mean $\pm$ *SD*), $1.16 \pm 0.04\%$, and $0.71 \pm 0.02\%$ for Positions 1, 2, and 3, respectively. A one-way repeated-measures ANOVA was performed for each dependent variable to assess the effect of Target Position. For hit rates, there was no main effect of Target Position, $F(1, 14) = 2.52$, $p = .09$, $\eta^2 = 15.29$. For median RTs, there was also no main effect of Target Position, $F(1, 14) = 1.24$, $p = .30$, $\eta^2 = 8.16$. For target contrast, there was a main effect of Target Position, $F(1, 14) = 13.68$, $p < .01$, $\eta^2 = 49.42$, which is coherent with the staircase manipulation.

Luminance Binning

Targets were binned according to the level of luminance of the simultaneously presented disk. To emulate an oscillatory cycle (which, in the main experiment, goes from 0% contrast to 100% and back to 0%), we used a bootstrap procedure (5000 repetitions) randomly assigning half of the targets to one half of the cycle (from 0% to 100% contrast), whereas the other half was assigned to the second half of the cycle (from 100% to 0% contrast), thus resulting in 13 luminance levels.

The number of false alarms (i.e., participants responded a target was present while it was absent) and the number of hits were computed for each target position and for the 13 luminance levels. A one-cycle sine function was fitted to individual data and data averaged across participants (Equation 2) with the following free parameters: the amplitude, $x[1]$; the phase offset, $x[2]$; and the baseline, $x[3]$. A least squares cost function was used to find the parameters that best fit the data.

$$x[1] \times \left(\sin(2 \times \pi \times T + x[2]) \right) + x[3] \qquad (2)$$

We performed a Monte Carlo procedure on the fitted amplitudes to assess whether the fitted data were modulated periodically by the luminance disk (see Statistical Analyses section). There was no significant effect of Luminance, at any target position, for the false alarm ratio, and thus we did not consider this variable any further.

The optimal phase, that is, phase of highest performance, was computed for each target position on data averaged across participants. To study whether the

optimal phase shifted as a function of target positions, we compared the individual optimal phase and assessed the significance using a one-way repeated-measures ANOVA (main variable: Individual Optimal Phase; main factor: Target Positions).

Control Experiment 2: Broadband Oscillating Disk

Experimental Design

Targets were of the same size and location as in the main experiment and Control Experiment 1. The peripheral disk was, however, oscillating in luminance with a broadband frequency profile centered on 10 Hz (from 4.1 to 23.9 Hz, excluding 10 Hz). This manipulation allowed testing potential masking effects under the same attentional condition as in the main experiment (note that, in the previous control, the flashing disk could have attracted attention in the periphery). Following the same staircase procedure as in the main experiment, participants then performed three runs of 42 blocks each, over two separate experimental sessions of ~1 hr 30 min each. In one of the two sessions of two of the participants, EEG was simultaneously recorded (same analysis as in the main experiment, see EEG Analysis above).

Analyses

Hit rates, median RTs, and target contrasts were computed for each target position. Hit rates were $46.1 \pm 1.11\%$ (mean $\pm$ *SD*), $44.68 \pm 1.22\%$, and $46.9 \pm 0.96\%$ for Positions 1, 2, and 3, respectively. Median RTs were 515 ± 9 msec (median $\pm$ *SD*), 520 ± 9 msec, and 515 ± 8 msec for Positions 1, 2, and 3, respectively. Target contrasts were $3.7 \pm 0.55\%$ (mean $\pm$ *SD*), $2.2 \pm 0.26\%$, and $2.29 \pm 0.28\%$, for Positions 1, 2, and 3, respectively. A one-way repeated-measures ANOVA was performed for each dependent variable to assess the effect of Target Position. There was no main effect of Target Position for both hit rates, $F(1, 14) = 3.45$, $p = .05$, $\eta^2 = 19.8$, and median RTs, $F(1, 14) = 1.13$, $p = .34$, $\eta^2 = 7.44$. For target contrast, there was a main effect of Target Position, $F(1, 14) = 23.95$, $p < .01$, $\eta^2 = 63.11$, which is coherent with the staircase manipulation.

Luminance Binning

Data were analyzed following the same procedure described in the Control Experiment 1: Flashing Disk section (see Luminance Binning section). Targets were binned according to the level of luminance of the oscillating disk, that is, seven equally spaced bins from 0% to 100% levels of contrast followed by a bootstrap procedure to obtain 13 luminance levels. A one-cycle sine function was fitted to individual data and data averaged across participants (Equation 2), and a least squares cost function was used to find the parameters that best fit the data. A

Monte Carlo procedure on the fitted amplitudes was performed to assess whether the fitted data were modulated periodically by the luminance disk. Differences in optimal phase across target position were tested with a one-way repeated-measures ANOVA (main variable: Individual Optimal Phase; main factor: Target Positions).

Luminance Peak Binning

To assess whether the maximal luminance of the peripheral disk could induce behavioral masking, which would then propagate across the retinotopic space, targets were assigned to time bins of 100-msec periods after the peaks in disk luminance. Here again, a one-cycle sine function (Equation 2) was fitted to the data, and a Monte Carlo procedure assessed significance. Differences in optimal phase across target position were tested with a one-way repeated-measures ANOVA (main variable: Individual Optimal Phase; main factor: Target Positions).

Pseudophase Binning

To assess whether the arrhythmic, broadband (around, but not including, 10 Hz) peripheral disk produced the same results as in the main experiment in which the disk is oscillating at 10 Hz, targets were assigned to phase bins of 100-msec periods starting from disk onset. As before, a one-cycle sine function was fitted to individual data and data averaged across participants (Equation 2), and a Monte Carlo procedure on the fitted amplitudes was performed to test whether the data were modulated at 10 Hz.

Statistical Analyses

To test whether the fitted data were significantly modulated periodically by the phase of the oscillating disk (see Phase Effect on Detection Performance section), a Monte Carlo procedure on the fitted amplitude was performed. Fifty thousand surrogates were generated for each participant, target position, and frequency, by randomly assigning correct responses (for each target, we randomly assigned an incorrect or correct response based on the averaged performance) and false alarms (a number of false alarms at an associated random delay were randomly assigned to each block, based on the average number of false alarms throughout the experiment). Hit and false alarm rates were then computed for each phase bin, position, and frequency, and the same sine function was fitted (Equation 1). The surrogate distributions of the 50,000 fitted amplitudes for the induced frequency (free parameter $x[1]$ from Equation 1) and the first harmonic (free parameter $x[3]$ from Equation 1) were compared to the empirical fitted amplitudes; that is, the surrogate fitted amplitudes of each component (induced, first harmonic, sum of both) were respectively compared to the empirical fitted amplitudes. p Values were obtained by computing the proportion of fitted amplitudes equal to

or higher than the empirical fitted amplitude (fitted amplitudes: free parameters $x[1]$ and $x[3]$ from Equation 1). The fitted amplitudes of the induced frequency ($x[1]$) and of the first harmonic ($x[3]$) across all frequencies and target positions were compared with a two-tailed t test to investigate which frequency contributes the most to the oscillatory pattern.

In the control experiments (see Control Experiment section), the same Bonferroni-corrected Monte Carlo procedures were performed, except that the 50,000 data sets were created for each binning condition and that the sine function (Equation 2) was fitted to the data.

RESULTS

Participants ($n = 17$) performed a threshold visual detection task, while a luminance oscillating disk was concurrently presented in the periphery (eccentricity: 7.5°) to modulate perception at the theta and alpha frequencies (4, 6, 8, and 10 Hz; EEG simultaneously recorded). Near-threshold target stimuli appeared at one of three possible eccentricities between a central fixation cross and the disk (Figure 1A; adjusted according to cortical magnification so each target measured 0.8 mm of diameter and were placed 0.8 mm away from each other in the cortex; see Figure 1B). We tested whether (1) the periodic disk stimulation modulates detection performance periodically at each target position, (2) the optimal phase (of highest performance) shifts as a function of distance from the disk suggesting that induced perceptual cycles travel across space (Figure 1C), and (3) the occurrence of such traveling properties depends on the induced frequency.

EEG activity was analyzed using frequency decomposition (FFT performed on the time series of each participant and electrode) and ERP measures to ensure that we successfully induced frequency-specific brain activity and to characterize the shape of the evoked response. First, peaks in the spectrum (as measured per SNR, averaged across participants and electrodes) were identified for each induced frequency (4, 6, 8, and 10 Hz; SNR > 1.4) and their first harmonics (8, 12, 16, and 20 Hz; SNR > 1.57), with topographies showing brain activity in the occipital cortex (for simplicity, frequencies were rounded to a whole number; real values are displayed in Figure 2, left side of A–D). Second, ERP analyses showed that the evoked signal is a complex signal composed of the induced frequency and its first harmonic (Figure 2, right side of A–D). We further computed an FFT on the ERPs of electrode Oz. Peaks were again identified for each induced frequency (4, 6, 8, and 10 Hz; SNR > 2.4) and their first harmonics (8, 12, 16, and 20 Hz; SNR > 4.41; data not shown). Note that both SNR computed on EEG time series and on EEG evoked activity are >1 for each induced frequency and first harmonic demonstrating that the disk induced frequency-specific brain activity. These complex evoked responses were interpreted as the overlap between the periodic brain response (i.e., inducer) and
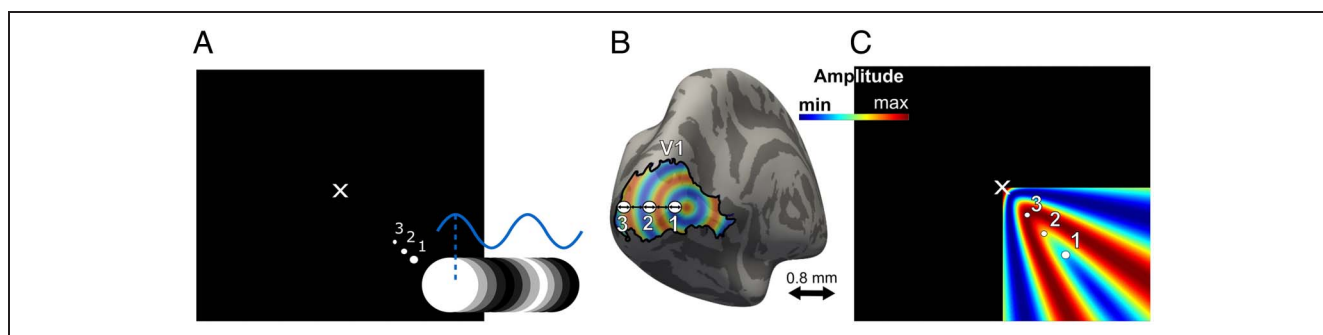
Figure 1. Experimental protocol. (A) A luminance oscillating disk (inducer) was presented in the periphery to induce perceptual cycles at the theta and alpha frequency. Participants were instructed to detect visual targets at threshold (50% detection) at three different positions in the retinotopic space, based on cortical magnification. Disks oscillated for a 30-sec period during which 6–18 targets were presented at random times according to a decreasing probability distribution. Participants pressed the space bar when they detected the target (1-sec response window after target onset). (B) In the visual cortex, visual targets measured 0.8 mm in diameter and were placed 0.8 mm away from each other. (C) Hypothesis: The oscillating disk, presented in the lower right corner, induced a brain activity that traveled across the retinotopic space (note that we concentrate our predictions to the quadrant in which the disk is presented). At an instant *t*, Position 3 is located at the maximum (max) amplitude of the induced brain activity, leading to the highest performance, whereas Position 1 is located at the minimum (min) amplitude.

the neural population response to individual stimuli (i.e., contrast change) at low frequencies or, alternatively, to the nonlinear nature of the visual system; that is, nonlinear systems produce complex output consisting of the input

frequency and multiple harmonics (Norcia, Appelbaum, Ales, Cottereau, & Rossion, 2015; Heinrich, 2010). Together, the EEG analyses confirm that we successfully induced theta/alpha activity in the visual cortex and show
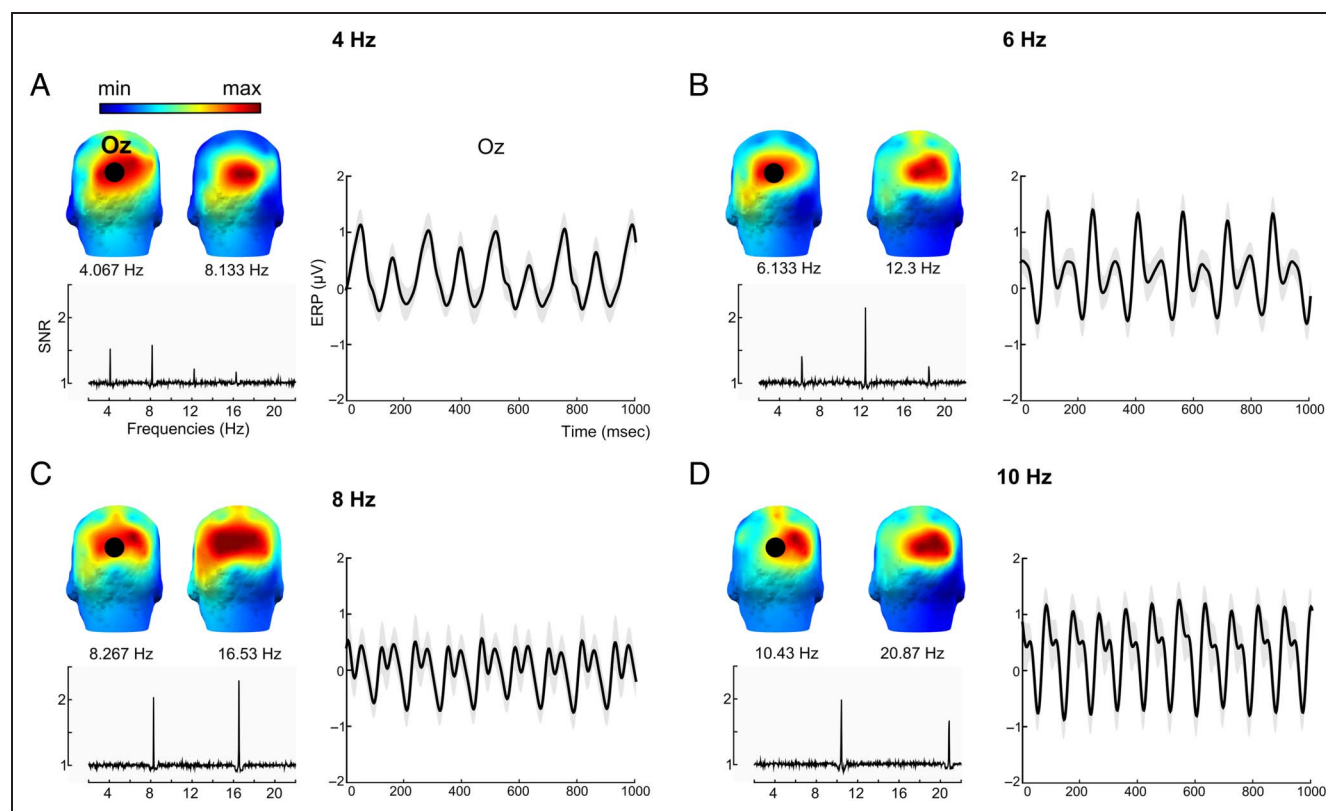

Figure 2. The oscillating disk induced frequency-specific brain activity in the occipital cortex. The left side of A–D shows FFT analyses performed on the EEG time series. The right side of A–D shows ERP analyses, for induced frequencies of (A) 4, (B) 6, (C) 8, and (D) 10 Hz (rounded frequency values). SNR amplitude averaged across 17 participants and all 62 electrodes, from 2 to 22 Hz. In each part of the figure, a peak in SNR is identified for the induced frequency and its first harmonic. Topographies of the two SNR peaks revealed that we successfully induced brain activity in the visual cortex. Black dots indicate electrode Oz. ERP of the Oz electrode computed on 1-sec epochs (the first-second epoch was removed to each 30-sec block to avoid the EEG transient evoked response; each block represented twenty-nine 1-sec epochs) averaged across participants (*n* = 17). Solid black lines indicate averaged ERP. Shaded areas indicate *SEM*. max = maximum; min = minimum.

that the evoked signal is a complex signal composed of the induced frequency and its first harmonic (Norcia et al., 2015; Heinrich, 2010).

Second, we investigated whether detection performance was modulated periodically for each induced frequency and each target position. Targets (from 6 to 18 targets per 30-sec block) can appear at random delays during the periodic disk stimulation (from 1 to 29 sec from disk onset). Targets were binned according to the phase of the oscillating disk (seven bins/cycle; least number of bins to sample one oscillatory period while allowing a large number of trials per bin to achieve high statistical power). In each bin, detection performance was computed as per hit rate (correct target detection) for each participant, frequency, and target position. Finally, the data were averaged across participants and, given the complex shape of the ERP (Figure 2), fit to a complex sine function (the shape of the evoked response was used as proxy for the shape of the behavioral response), separately for each frequency and target position. Detection performance showed a significant oscillatory pattern for each target position and frequency (Monte Carlo on fitted amplitude, Bonferroni corrected across frequencies and positions, p value threshold < .004, corresponding to a z score threshold of 2.64 and a Cohen's d threshold of 1.66; Figure 4) and a clear optimal phase (of highest performance). Note that the fitted amplitude of the induced frequency was significantly higher than the one of the first harmonic (two-tailed t test on fitted amplitude across all frequencies and positions, $p < .01$, Cohen's $d = 0.67$, 95% CI [0.05, 0.1]). A high fitted amplitude indicates that the fitted sine function explains a large portion of the variance in the behavioral performance. The results thus suggest that the oscillatory pattern was mainly driven by the induced frequency across all tested target positions and frequencies. The inducer modulated detection performance periodically, at each target position and at each frequency, with an average amplitude modulation (optimal-to-nonoptimal hit rate difference) of 42.71 ± 3.37%. The amplitude modulation was further computed for each participant, frequency, and target position (Figure 3). A two-way repeated-measures ANOVA revealed a significant main effect of Frequency, $F(3, 48) = 23.85$, SS = 0.67, $p < .01$, $\eta^2 = 59.85$, and no main effect of Target Position, $F(2, 32) = 0.9$, SS = 0.01, $p = .41$, $\eta^2 = 5.33$, nor of their interaction, $F(6, 96) = 0.92$, SS = 0.03, $p = .48$. The amplitude modulation was of 49.84 ± 3.45% for 4 Hz, 46.56 ± 3.57% for 6 Hz, 39.04 ± 2.67% for 8 Hz, and 35.39 ± 2.54% for 10 Hz. Post hoc two-tailed t tests showed that the amplitude modulation was higher for 4 Hz compared to 8 Hz ($p < .01$, Cohen's $d = 0.84$, 95% CI [0.07, 0.14]) and 10 Hz ($p < .01$, Cohen's $d = 1.15$, 95% CI [0.1, 0.18]), with a tendency compared to 6 Hz ($p = .06$, Cohen's $d = 0.22$, 95% CI [−0.01, 0.06]); higher for 6 Hz compared to 8 Hz ($p < .01$, Cohen's $d = 0.57$, 95% CI [0.04, 0.1]) and 10 Hz ($p < .01$, Cohen's $d = 0.87$, 95% CI [0.07, 0.14]); and higher for 8 Hz compared to 10 Hz ($p = .02$, Cohen's $d = 0.33$, 95% CI [0.01, 0.06]).
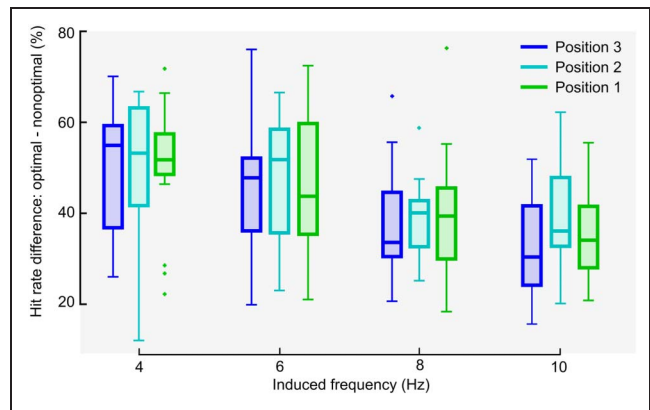

Figure 3. The amplitude modulation decreased with increasing induced frequency. Amplitude computed as the difference between the maximum and minimum hit rate. Dots indicate individual outlier data. A two-way repeated-measures ANOVA revealed a significant main effect of Frequency, $F(3, 48) = 23.85$, SS = 0.67, $p < .01$, $\eta^2 = 59.85$.

In summary, the amplitude modulation decreases with increasing frequency but is constant across target positions. The amplitude modulation allowed to reliably estimate the optimal phase at each frequency and target position. A complementary analysis showed that behavioral performance was better explained when taking into account the spatial position of the targets. Specifically, we compared the amplitude modulation when detection performance was calculated disregarding target position, with the amplitude modulation calculated independently for each target position and then averaged across positions (two-tailed t tests Bonferroni corrected for multiple comparisons: 4 Hz, t-stat = −5.84, $p < .01$, Cohen's $d = −0.3$, 95% CI [−0.05, −0.02]; 6 Hz, t-stat = −5.45, $p < .01$, Cohen's $d = −0.25$, 95% CI [−0.04, −0.02]; 8 Hz, t-stat = −5.35, $p < .01$, Cohen's $d = −0.3$, 95% CI [−0.04, −0.01]; 10 Hz, t-stat = −9.1, $p < .01$, Cohen's $d = −0.52$, 95% CI [−0.05, −0.03]). The amplitude modulation was significantly stronger when calculated position-by-position, suggesting that taking into account the spatial position of visual targets better explains perceptual performance.

Critically, we tested whether (1) perceptual cycles propagate across the retinotopic space and (2) the occurrence of such traveling properties depends on the induced frequency. Propagation is defined as a shift in the optimal phase between two positions. To assess whether the optimal phase shifted as a function of target position, individual optimal phases were converted in radians based on a one-cycle sine wave fit (see Methods section) at the induced frequency (the oscillatory pattern was mainly driven by the induced frequency; see analysis above). A Harrison–Kanji test revealed a significant main effect of Frequency, $F(3,48) = 25.13$, SS = 14.33, $p < .01$, and Target Position, $F(2,32) = 3.06$, SS = 1.16, $p = .04$, and a tendency for their interaction, $F(6,96) = 1.99$, SS = 2.42, $p = .06$. For the post hoc analyses, we performed
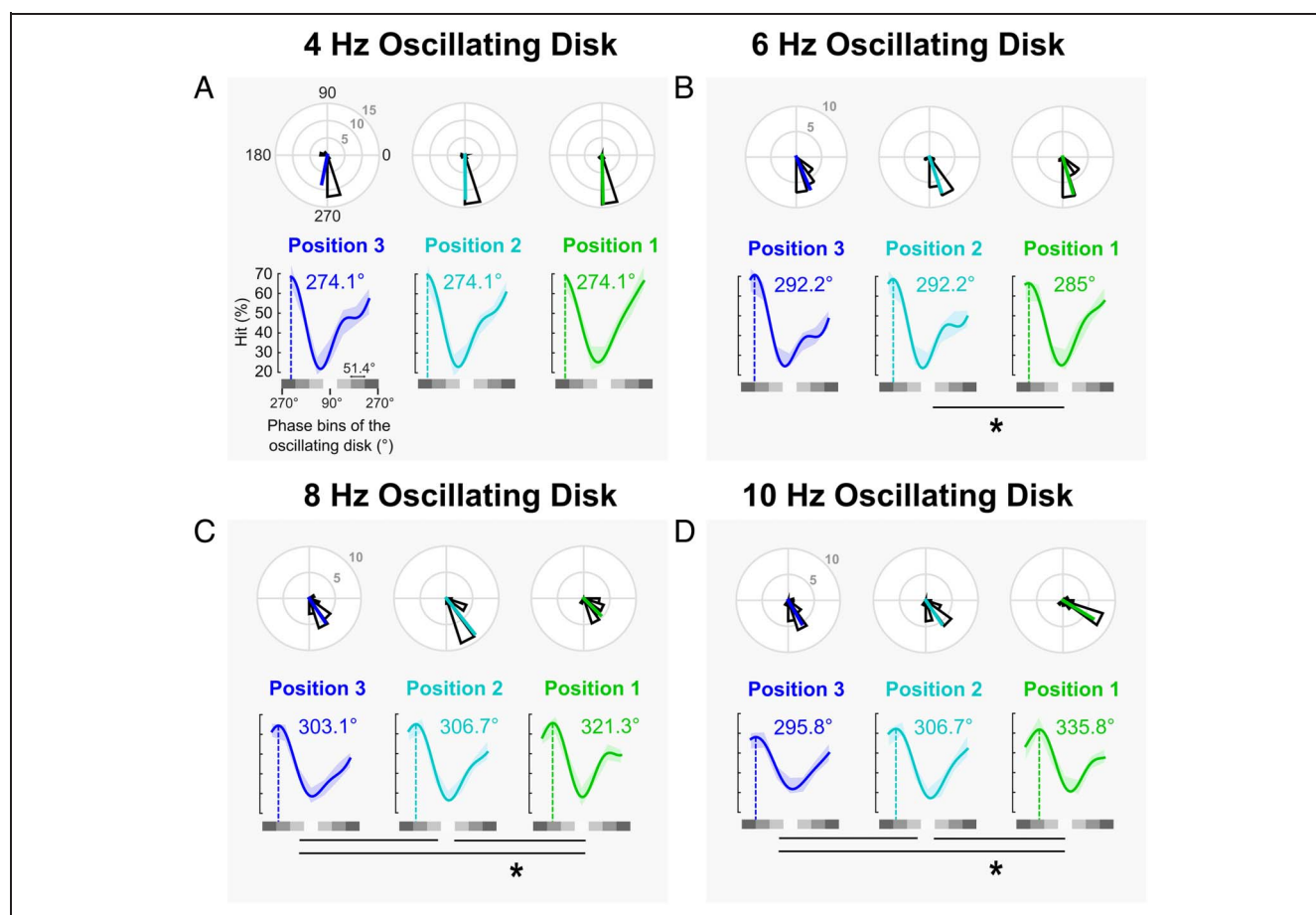
Figure 4. The optimal phase of alpha perceptual cycles shifts between target positions. The lower graphs of A–D show hit rates averaged across participants ($n = 17$), binned as a function of the phase of the oscillating disk, and fitted to a complex sine function. Shaded colored areas indicate 95 confidence intervals. Solid lines indicate sine fit. Dotted lines indicate optimal phase in degrees. The value of the optimal phase in degrees is extracted for fit on data averaged across participants (note that this closely resembles the value obtained from averaging individual optimal phases from the top graph). The top graphs of A–D show rose plot distribution of the optimal phase across participants. Colored solid lines indicate optimal phase averaged across participants. Gray scales indicate phase bins of the oscillating disk (90°, white disk). Each bin represents 51.4° of the oscillatory cycle. (A) Results for induced frequencies of (A) 4, (B) 6, (C) 8, and (D) 10 Hz. Performance was significantly modulated periodically at each target position and frequency (Monte Carlo, Bonferroni corrected across target positions and frequencies, p value threshold $< .01$). The optimal phase shifted between Positions 1 and 2, Positions 2 and 3, and Positions 1 and 3 for 8- and 10-Hz induced frequencies and between Positions 1 and 2 for 6-Hz induced frequency (Watson–Williams test, Bonferroni corrected across target positions and frequencies, * : p value threshold $< .004$). There was no significant phase shift for the 4-Hz induced frequency.

Watson–Williams tests against 0, that is, null difference, on participant-by-participant pairwise phase differences, for each pair of positions (Positions 1 and 2, Positions 1 and 3, and Positions 2 and 3). The results showed a significant phase shift between Positions 1 and 2, Positions 1 and 3, and Positions 2 and 3, for both 8 and 10 Hz (Figure 4C and D; Bonferroni corrected across frequencies and positions, $p < .004$), and between Positions 1 and 2 for 6 Hz. Thus, we did not find a systematic phase shift, that is, phase shift between each target position, for 4 and 6 Hz (Figure 4A and B). Together, the results demonstrate that the behavioral optimal phase of alpha perceptual cycles shifted across target positions, suggesting that brain signals traveled across the retinotopic cortical space. In addition, the phase shift cannot be explained by a decreased phase estimation accuracy at low frequencies (see Figure 3, showing that the amplitude modulation

is in fact higher at low compared to high induced frequency).

When converting the phase shift observed between target positions into milliseconds (3 msec for 8 Hz and 5.5 msec for 10 Hz, respectively) and given the cortical distance between two target positions (0.8-mm distance, edge-to-edge) as well as the targets' cortical size (0.8-mm diameter), one can estimate that alpha-induced brain oscillations traveled across the retinotopic space at an averaged propagation speed ranging between 0.3 m/sec (1.6 mm/ 5.5 msec) and 0.5 m/sec (1.6 mm/3 msec).

Finally, one may ask whether the phase shift observed in behavioral data was because of luminance masking from the disk. We performed two control experiments (15 participants each) to address this potential concern. Participants were instructed to detect visual targets at threshold (50% detection) at one of the same three positions as in

the main experiment, while a peripheral disk was simultaneously flashed at one of seven possible levels of luminance (see Control Experiment 1: Flashing Disk section; same as Sokoliuk & VanRullen, 2016), or while the disk was oscillating in luminance with an arrhythmic broadband frequency profile centered on 10 Hz (Control Experiment 2: Broadband Oscillating Disk section). First, for both control experiments, detection performance was calculated for each level of luminance, and a one-cycle sine function was fitted to the empirical data (see Luminance Binning sections under Control Experiment 1 and Control Experiment 2). For both control conditions, detection performance showed a significant oscillatory pattern at each target position (Monte Carlo, Bonferroni corrected across positions, p value threshold of .01, corresponding to a z score threshold of 2.12 and a Cohen's d threshold of 1.31; Figure 5A and B), confirming the presence of luminance masking at all three positions. We then compared the individual optimal phase between target positions. There was no significant phase shift in both the flashing disk control, $F(2, 14) = 1$, SS = 345.5, $p = .38$, $\eta^2 = 6.67$, and the broadband oscillating disk control, $F(2, 14) = 0$, SS = 3.61, $p = .99$, $\eta^2 = 0$, suggesting that the propagation of perceptual cycles observed in the main experiment was not because of masking.

To further investigate whether the maximal luminance of the disk (100% contrast) could induce a propagation of behavioral masking, targets in the broadband oscillating disk experiment were binned as a function of the peak luminance (see Luminance Peak Binning section). Visual performance showed a significant oscillatory modulation for Positions 1 and 2 (Monte Carlo, Bonferroni corrected across positions, p value threshold of .01, corresponding to a z score threshold of 2.12 and a Cohen's d threshold of 1.31) but not Position 3 ($p = .04$, above the Bonferroni-corrected p value threshold; Figure 5C). Although the fluctuation was not significant at Position 3, we still compared the individual optimal phases between
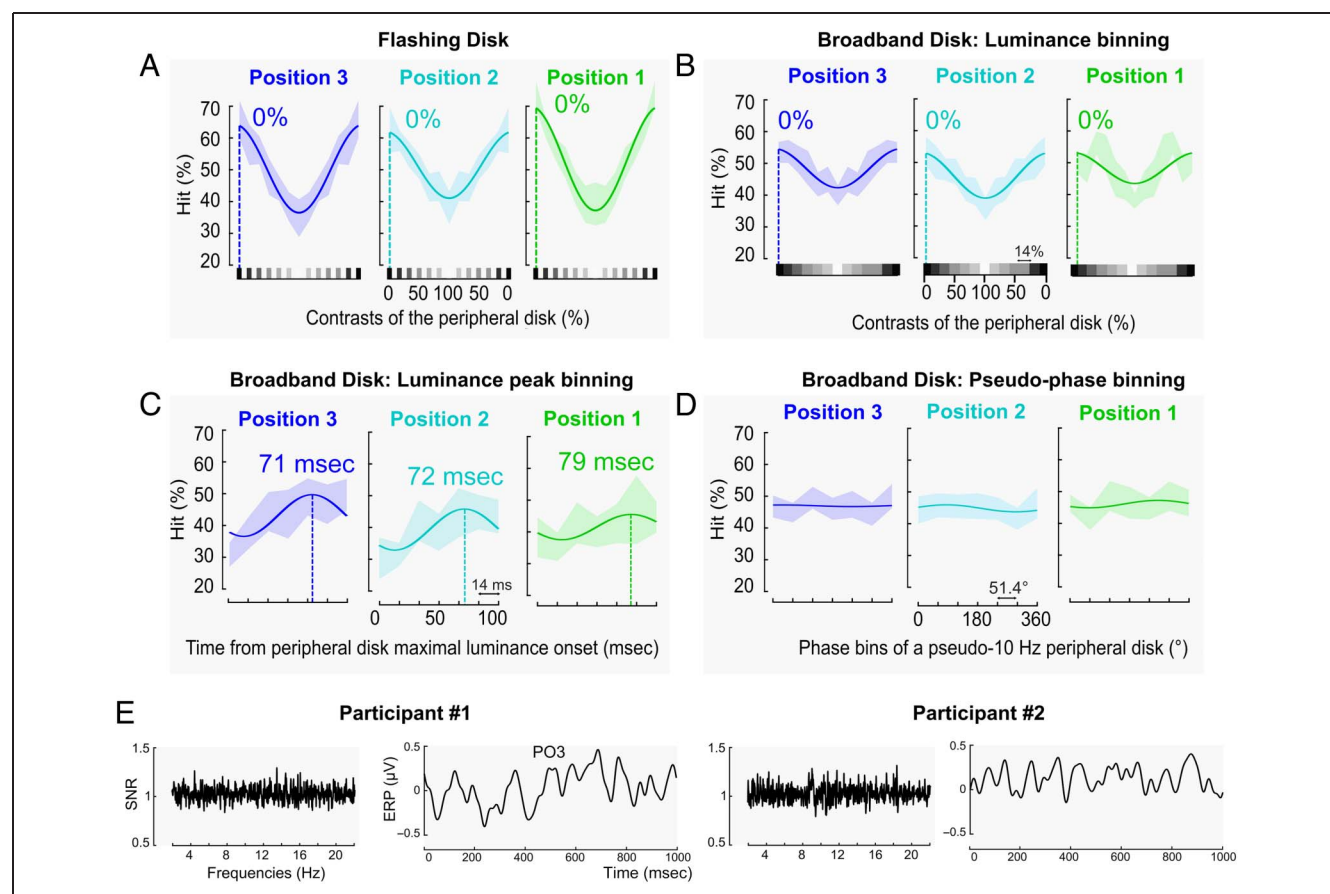

Figure 5. The propagation of induced perceptual cycles was not because of luminance masking. (A) Flashing disk control: hit rate for each of the 13 discrete luminance levels and three target positions averaged across participants ($n = 15$) and fitted to a one-cycle sine function. Shaded color areas indicate 95 confidence intervals. Solid lines indicate fit. Dotted lines indicate optimal behavioral phase. Green: Position 1, cyan: Position 2, blue: Position 3. (B) Broadband oscillatory disk control: hit rate for each of 13 luminance bins and three target positions averaged across participants ($n = 15$) and fitted to a one-cycle sine function. (C) Hit rate for each of the seven time bins from the peripheral disk maximal luminance onset and the three target positions averaged across participants ($n = 15$) and fitted to a one-cycle sine function. (D) Hit rate for each of the seven pseudophase bins of 10-Hz rhythmic modulation and the three target positions averaged across participants ($n = 15$) and fitted to a one-cycle sine function. (E) EEG data of two individual participants. The graphs on the left side show SNR amplitude averaged across all 62 electrodes on the FFT performed on the EEG time series. The graphs on the right side show ERP of the PO3 electrode computed on 1-sec epochs (the first-second epoch was removed to each 30-sec block to avoid the EEG transient evoked response; each block represented twenty-nine 1-sec epochs).

target positions. The test did not reveal a significant phase shift, $F(2, 14) = 0.7$, SS = 590.93, $p = .5$, $\eta^2 = 4.82$. Coherent with the previous result, although the disk maximal luminance masked visual performance of nearby targets, this masking cannot explain the shift of the optimal phase in the main experiment.

We finally investigated whether the arrhythmic, broadband peripheral disk produced the same results as in the main experiment by binning the targets every 100 msec (see Pseudophase Binning section). Although centered at 10 Hz, the broadband oscillating disk did not periodically modulate detection performance at 10 Hz (Monte Carlo, $p > .44$; Figure 5D). This absence of rhythmic modulation was coherent with the EEG analysis on two participants showing that the broadband peripheral disk did not evoke a frequency-specific 10-Hz brain activity (see SNR results on Figure 5E; although it did induce broadband activity around 10 Hz, analysis was not shown). In other words, the broadband visual stimulation did not induce narrowband 10-Hz brain activity, coherent with the behavioral results showing no alpha-induced perceptual cycle.

Taken together, the results of both control experiments show that the phase shift observed in the main experiment cannot be merely explained by low-level luminance masking (Figure 5).

DISCUSSION

Using psychophysics and EEG, we showed that visual perception at each target position is modulated periodically at the induced frequency, replicating previous results (Kizuk & Mathewson, 2017; Ten Oever & Sack, 2015; Henry et al., 2014; Spaak et al., 2014; De Graaf et al., 2013; Henry & Obleser, 2012; Mathewson et al., 2012; Stefanics et al., 2010). Critically, the optimal phase for visual perception systematically shifted between target positions. This effect was observed for alpha-induced frequencies (8 and 10 Hz; and cannot be simply explained by a mere luminance masking confound), and not theta, with an average propagation speed ranging from 0.3 to 0.5 m/sec. Together, the results support the hypothesis that induced perceptual cycles propagate across the retinotopic visual space presumably because of horizontal connections in the retinotopic visual cortex.

Entrained Oscillations or Periodic Evoked Response?

Our results showed that perceptual cycles are propagating across the visual retinotopic space, suggesting that the underlying neural activity is propagating as well in the cortical retinotopic space through horizontal axons. We cannot, however, conclude whether this propagating activity corresponds to the propagation of true entrained oscillations or of a succession of evoked responses. Our EEG recordings highlighted that the evoked signal was composed of the induced frequency and its first harmonic, interpreted as the overlap between the periodic brain response

(i.e., inducer) and the neural population response to individual stimuli (i.e., contrast change) at low frequencies, or alternatively, to the nonlinear nature of the visual system; that is, nonlinear systems produce complex output consisting of the input frequency and multiple harmonics (Norcia et al., 2015; Heinrich, 2010). The propagation we observed in this study being frequency band specific, we argue that the most parsimonious interpretation is to consider entrained brain oscillations. However, and regardless of the underlying cortical mechanism, whether entrained oscillations or periodic ERPs, our conclusions remain unchanged; that is, induced perceptual cycles propagate across the retinotopic space.

Propagation of Alpha but not Theta Perceptual Cycles

Attention is the cognitive function that selects relevant information to facilitate its processing while still being able to flexibly redeploy resources to other information if necessary (Dugué et al., 2018, 2020; Carrasco, 2011). Studies have shown that when covert attention (no head/eye movements) is sustained at a given spatial location, information is sampled periodically at the alpha frequency (for a review, see Kienitz et al., 2022; Dugué & VanRullen, 2017). In other words, visual performance fluctuates over time in the alpha band in detection tasks in which the target stimulus appeared always at the same spatial location (Fakche et al., 2022; Samaha et al., 2017; Samaha & Postle, 2015; Dugué et al., 2011; Busch & VanRullen, 2010; Busch et al., 2009; Mathewson et al., 2009; Valera et al., 1981). However, when multiple stimuli are presented, attention rhythmically samples information at the theta frequency (Galas, Donovan, & Dugué, 2023; Merholz, Grabot, VanRullen, & Dugué, 2022; Dugué, Beck, Marque, & VanRullen, 2019; Dugué et al., 2015; Huang et al., 2015; Song et al., 2014; Fiebelkorn, Saalmann, et al., 2013; Landau & Fries, 2012; see also Re et al., 2023; Keitel, Ruzzoli, Dugué, Busch, & Benwell, 2022; Kienitz et al., 2022; Dugué & VanRullen, 2017; VanRullen, 2016, for reviews).

Here, although we did not explicitly manipulate covert attention, participants fixated at the center of the screen and targets appeared in a constrained location suggesting that covert, voluntary spatial attention was sustained on the bottom right quadrant. This manipulation likely recruited alpha sampling, which potentially favored the propagation of alpha-induced perceptual cycles. One can speculate that the propagation of alpha perceptual cycles away from the main attention focus could allow the observer to periodically monitor other nearby locations allowing for flexible attentional reallocation when a target appears. Further studies are necessary to investigate this hypothesis.

Perceptual Propagation Suggests Cortical Propagation

Sokoliuk and VanRullen (2016) reasoned that if an induced brain activity propagates across the visual cortex, it should

have perceptual consequences across the retinotopic visual space. Using a similar psychophysical paradigm, they found a shift of the behavioral optimal phase as a function of distance from the inducer. Yet, there are two notable differences between their study and the present one. First, they observed that the phase shifted between the visual stimulus closest to the inducer and more distant ones (no differences between intermediate positions). Yet, postulating brain activity is traveling within the cortex requires showing a phase change across all positions. Here, contrary to Sokoliuk and VanRullen (2016), we found a systematic phase shift across all three positions.

Second, Sokoliuk and VanRullen (2016) observed an optimal phase shift for both induced frequencies of 5 Hz (theta) and 10 Hz (alpha), but not 15 Hz. Here, however, we showed a shift for alpha-induced frequencies (8 and 10 Hz), but not theta (4 and 6 Hz).

Together, these discrepant results can be explained by a number of critical differences between the two studies. First, the EEG analysis confirmed that the oscillating disk induced frequency-specific brain activity in the occipital cortex. This result was important to validate our rationale postulating that induced perceptual cycles travel across the visual retinotopic space because of the propagation of brain activity across the cortical retinotopic space. Importantly, our EEG results revealed that the oscillating disk produced a complex neural response composed of the induced frequency and its first harmonic, coherent with the nature of the visual system (Norcia et al., 2015; Spaak et al., 2014; Heinrich, 2010). Thus, one must fit the behavioral response with a corresponding complex sine function to accurately capture the nonlinearity of the neural response. Because the EEG was not recorded in Sokoliuk and VanRullen (2016), the shape of the induced brain signal was unknown. Second, to ensure that the three targets activated the same number of neurons in visual regions, hence landing in a similar spatial extent (spatial phase) of the propagating activity, we adjusted the size of each target to cortical magnification. Third, in our study, the same participants ($n = 17$) performed all four frequency conditions, thus ensuring equal statistical power and no interindividual variability ($n = 5$ for 5 Hz, $n = 7$ for 10 Hz, $n = 15$ for a 10-Hz replication set, and $n = 4$ for 15 Hz in Sokoliuk & VanRullen, 2016). Finally, we used eye tracking to ensure stable fixation, critical when investigating retinotopic propagation.

Neural Mesoscopic Traveling Waves, a Growing, yet Largely Understudied Field

A traveling wave is the propagation of neural activity over space with a monotonic shift in the peak latency between the origin of the signal and more distal positions (Muller, Chavane, Reynolds, & Sejnowski, 2018; Sato, Nauhaus, & Carandini, 2012).

Mesoscopic waves travel within individual brain regions (e.g., V1) spanning millimeters (Muller et al., 2018; Sato

et al., 2012). Studies using invasive recordings with high spatial and temporal resolution showed nonoscillatory traveling activity in visual cortices of mammals (Chemla et al., 2019; Rekauzke et al., 2016; Yang et al., 2015; Gao et al., 2012; Nauhaus, Busse, Ringach, & Carandini, 2012; Reynaud, Masson, & Chavane, 2012; Zhang et al., 2012; Nauhaus, Busse, Carandini, & Ringach, 2009; Sit, Chen, Geisler, Miikkulainen, & Seidemann, 2009; Takagaki, Zhang, Wu, & Lippert, 2008; Lippert, Takagaki, Xu, Huang, & Wu, 2007; Sharon, Jancke, Chavane, Na'aman, & Grinvald, 2007; Xu, Huang, Takagaki, & Wu, 2007; Chen, Geisler, & Seidemann, 2006; Roland et al., 2006; Jancke et al., 2004; Slovin, Arieli, Hildesheim, & Grinvald, 2002; Bringuier et al., 1999). Much fewer studies have focused on mesoscopic oscillatory traveling waves (spontaneous, entrained, or evoked). They showed that delta, theta, alpha, beta, and gamma oscillations can propagate within individual visual areas of mammals and turtles (Davis et al., 2020; Townsend et al., 2015; Zanos et al., 2015; Muller et al., 2014; Maris, Womelsdorf, Desimone, & Fries, 2013; Stroh et al., 2013; Ray & Maunsell, 2011; Han, Caporale, & Dan, 2008; Benucci et al., 2007; Huang et al., 2004; Prechtl, Bullock, & Kleinfeld, 2000; Sanchez-Vives & McCormick, 2000; Prechtl, Cohen, Pesaran, Mitra, & Kleinfeld, 1997). In humans, only a few studies, using invasive recordings in patients, showed the propagation of theta, alpha, and beta mesoscopic traveling waves (Sreekumar, Wittig, Chapeton, Inati, & Zaghloul, 2020; Zhang & Jacobs, 2015; Takahashi, Saleh, Penn, & Hatsopoulos, 2011), but only in nonvisual cortical areas. There is no electrophysiological study to date investigating the propagation of low-frequency oscillations in individual human visual areas (see Grabot, Merholz, Winawer, Heeger, & Dugué, 2022, for a computational solution).

Finally, if a few studies have investigated the functional role of propagating oscillatory activity at the mesoscopic levels (attention: Maris et al., 2013; memory: Han et al., 2008; motricity: Takahashi et al., 2011, 2015; Rubino, Robbins, & Hatsopoulos, 2006; saccadic eye movements: Zanos et al., 2015; visual perception: Davis et al., 2020; Besserve, Lowe, Logothetis, Schölkopf, & Panzeri, 2015), very little is known about the link between oscillatory activity propagation within individual visual areas and perceptual performance, especially in humans. The present study addresses this clear gap in the literature.

Speed and Spatial Extent of Mesoscopic Traveling Waves

Our results show that induced alpha perceptual cycles travel across the retinotopic space at a propagation speed ranging from 0.3 to 0.5 m/sec. Such observation is in line with results from the animal literature showing that low-frequency oscillations propagate within visual areas at a speed ranging from 0.01 to 0.6 m/sec (Davis et al.,

2020; Zanos et al., 2015; Muller et al., 2014; Ray & Maunsell, 2011; Han et al., 2008; Benucci et al., 2007; Prechtl et al., 2000; Sanchez-Vives & McCormick, 2000; Prechtl et al., 1997). In addition, given a phase difference of a maximum of 40° between target positions, it is unlikely that more than one (spatial) cycle (360°) of oscillatory activity propagates across such a small portion of the visual cortex, in line with previous observations (Zanos et al., 2015; Zhang & Jacobs, 2015).

Finally, given our specific contrast manipulation and the observed propagation of induced perceptual cycles, it is likely that our paradigm preferentially probed alpha traveling waves in area V1 (with small receptive fields).

Conclusion

Using a carefully designed psychophysical paradigm, combined with EEG and eye tracking, our study demonstrates that induced alpha perceptual cycles travel across the retinotopic visual space in humans, at a propagation speed ranging from 0.3 to 0.5 m/sec. These results suggest that brain activity travels across the visual cortex to modulate performance periodically across space and time.

Data Availability Statement

Raw behavioral data and code relative to the main results are available at github.com/CamilleFakche.

Diversity in Citation Practices

Retrospective analysis of the citations in every article published in this journal from 2010 to 2021 reveals a persistent pattern of gender imbalance: Although the proportions of authorship teams (categorized by estimated gender identification of first author/last author) publishing in the *Journal of Cognitive Neuroscience* (*JoCN*) during this period were M(an)/M = .407, W(oman)/M = .32, M/W = .115, and W/W = .159, the comparable proportions for the articles that these authorship teams cited were M/M = .549, W/M = .257, M/W = .109, and W/W = .085 (Postle and Fulvio, *JoCN*, 34:1, pp. 1–3). Consequently, *JoCN* encourages all authors to consider gender balance explicitly when selecting which articles to cite and gives them the opportunity to report their article's gender citation balance. The authors of this article report its proportions of citations by gender category to be as follows: M/M = .642, W/M = .221, M/W = .074, and W/W = .063.

REFERENCES

Baumgarten, T. J., Schnitzler, A., & Lange, J. (2015). Beta oscillations define discrete perceptual cycles in the somatosensory domain. *Proceedings of the National Academy of Sciences, U.S.A.*, *112*, 12187–12192. https://doi.org/10.1073/pnas.1501438112, PubMed: 26324922

Benucci, A., Frazor, R. A., & Carandini, M. (2007). Standing waves and traveling waves distinguish two circuits in visual cortex. *Neuron*, *55*, 103–117. https://doi.org/10.1016/j.neuron.2007.06.017, PubMed: 17610820

Berens, P. (2009). CircStat: A MATLAB toolbox for circular statistics. *Journal of Statistical Software*, *31*, 1–21. https://doi.org/10.18637/jss.v031.i10

Besserve, M., Lowe, S. C., Logothetis, N. K., Schölkopf, B., & Panzeri, S. (2015). Shifts of gamma phase across primary visual cortical sites reflect dynamic stimulus-modulated information transfer. *PLoS Biology*, *13*, e1002257. https://doi.org/10.1371/journal.pbio.1002257, PubMed: 26394205

Bringuier, V., Chavane, F., Glaeser, L., & Frégnac, Y. (1999). Horizontal propagation of visual activity in the synaptic integration field of area 17 neurons. *Science*, *283*, 695–699. https://doi.org/10.1126/science.283.5402.695, PubMed: 9924031

Busch, N. A., Dubois, J., & VanRullen, R. (2009). The phase of ongoing EEG oscillations predicts visual perception. *Journal of Neuroscience*, *29*, 7869–7876. https://doi.org/10.1523/JNEUROSCI.0113-09.2009, PubMed: 19535598

Busch, N. A., & VanRullen, R. (2010). Spontaneous EEG oscillations reveal periodic sampling of visual attention. *Proceedings of the National Academy of Sciences, U.S.A.*, *107*, 16048–16053. https://doi.org/10.1073/pnas.1004801107, PubMed: 20805482

Carrasco, M. (2011). Visual attention: The past 25 years. *Vision Research*, *51*, 1484–1525. https://doi.org/10.1016/j.visres.2011.04.012, PubMed: 21549742

Carrasco, M., & McElree, B. (2001). Covert attention accelerates the rate of visual information processing. *Proceedings of the National Academy of Sciences, U.S.A.*, *98*, 5363–5367. https://doi.org/10.1073/pnas.081074098, PubMed: 11309485

Chavane, F., Perrinet, L. U., & Rankin, J. (2022). Revisiting horizontal connectivity rules in V1: From like-to-like towards like-to-all. *Brain Structure and Function*, *227*, 1279–1295. https://doi.org/10.1007/s00429-022-02455-4, PubMed: 35122520

Chemla, S., Reynaud, A., di Volo, M., Zerlaut, Y., Perrinet, L., Destexhe, A., et al. (2019). Suppressive traveling waves shape representations of illusory motion in primary visual cortex of awake primate. *Journal of Neuroscience*, *39*, 4282–4298. https://doi.org/10.1523/JNEUROSCI.2792-18.2019, PubMed: 30886010

Chen, Y., Geisler, W. S., & Seidemann, E. (2006). Optimal decoding of correlated neural population responses in the primate visual cortex. *Nature Neuroscience*, *9*, 1412–1420. https://doi.org/10.1038/nn1792, PubMed: 17057706

Davis, Z. W., Muller, L., Martinez-Trujillo, J., Sejnowski, T., & Reynolds, J. H. (2020). Spontaneous travelling cortical waves gate perception in behaving primates. *Nature*, *587*, 432–436. https://doi.org/10.1038/s41586-020-2802-y, PubMed: 33029013

De Graaf, T. A., Gross, J., Paterson, G., Rusch, T., Sack, A. T., & Thut, G. (2013). Alpha-band rhythms in visual task performance: Phase-locking by rhythmic sensory stimulation. *PLoS One*, *8*, e60035. https://doi.org/10.1371/journal.pone.0060035, PubMed: 23555873

Delorme, A., & Makeig, S. (2004). EEGLAB: An open source toolbox for analysis of single-trial EEG dynamics including independent component analysis. *Journal of Neuroscience Methods*, *134*, 9–21. https://doi.org/10.1016/j.jneumeth.2003.10.009, PubMed: 15102499

Dugué, L., Beck, A.-A., Marque, P., & VanRullen, R. (2019). Contribution of FEF to attentional periodicity during visual search: A TMS study. *eNeuro*, *6*, ENEURO.0357-18.2019. https://doi.org/10.1523/ENEURO.0357-18.2019, PubMed: 31175148

Dugué, L., Marque, P., & VanRullen, R. (2011). The phase of ongoing oscillations mediates the causal relation between brain excitation and visual perception. *Journal of Neuroscience*, *31*, 11889–11893. https://doi.org/10.1523/JNEUROSCI.1161-11.2011, PubMed: 21849549

Dugué, L., Marque, P., & VanRullen, R. (2015). Theta oscillations modulate attentional search performance periodically. *Journal of Cognitive Neuroscience*, *27*, 945–958. https://doi.org/10.1162/jocn_a_00755, PubMed: 25390199

Dugué, L., Merriam, E. P., Heeger, D. J., & Carrasco, M. (2018). Specific visual subregions of TPJ mediate reorienting of spatial attention. *Cerebral Cortex*, *28*, 2375–2390. https://doi.org/10.1093/cercor/bhx140, PubMed: 28981585

Dugué, L., Merriam, E. P., Heeger, D. J., & Carrasco, M. (2020). Differential impact of endogenous and exogenous attention on activity in human visual cortex. *Scientific Reports*, *10*, 21274. https://doi.org/10.1038/s41598-020-78172-x, PubMed: 33277552

Dugué, L., & VanRullen, R. (2017). Transcranial magnetic stimulation reveals intrinsic perceptual and attentional rhythms. *Frontiers in Neuroscience*, *11*, 154. https://doi.org/10.3389/fnins.2017.00154, PubMed: 28396622

Fakche, C., VanRullen, R., Marque, P., & Dugué, L. (2022). α Phase-amplitude tradeoffs predict visual perception. *eNeuro*, *9*, ENEURO.0244-21.2022. https://doi.org/10.1523/ENEURO.0244-21.2022, PubMed: 35105658

Fiebelkorn, I. C., Saalmann, Y. B., & Kastner, S. (2013). Rhythmic sampling within and between objects despite sustained attention at a cued location. *Current Biology*, *23*, 2553–2558. https://doi.org/10.1016/j.cub.2013.10.063, PubMed: 24316204

Fiebelkorn, I. C., Snyder, A. C., Mercier, M. R., Butler, J. S., Molholm, S., & Foxe, J. J. (2013). Cortical cross-frequency coupling predicts perceptual outcomes. *Neuroimage*, *69*, 126–137. https://doi.org/10.1016/j.neuroimage.2012.11.021, PubMed: 23186917

Galas, L., Donovan, I., & Dugué, L. (2023). Attention rhythmically shapes sensory tuning. *BioRxiv*, *2023-05*, 1–21. https://doi.org/10.1101/2023.05.26.542055

Gao, X., Xu, W., Wang, Z., Takagaki, K., Li, B., & Wu, J.-Y. (2012). Interactions between two propagating waves in rat visual cortex. *Neuroscience*, *216*, 57–69. https://doi.org/10.1016/j.neuroscience.2012.04.062, PubMed: 22561730

Girard, P., Hupé, J. M., & Bullier, J. (2001). Feedforward and feedback connections between areas V1 and V2 of the monkey have similar rapid conduction velocities. *Journal of Neurophysiology*, *85*, 1328–1331. https://doi.org/10.1152/jn.2001.85.3.1328, PubMed: 11248002

Grabot, L., Merholz, G., Winawer, J., Heeger, D., & Dugué, L. (2022). Computational modeling of traveling waves using MEG–EEG in human. *Journal of Vision*, *22*, 3511. https://doi.org/10.1167/jov.22.14.3511

Han, F., Caporale, N., & Dan, Y. (2008). Reverberation of recent visual experience in spontaneous cortical waves. *Neuron*, *60*, 321–327. https://doi.org/10.1016/j.neuron.2008.08.026, PubMed: 18957223

Hanslmayr, S., Volberg, G., Wimber, M., Dalal, S. S., & Greenlee, M. W. (2013). Prestimulus oscillatory phase at 7 Hz gates cortical information flow and visual perception. *Current Biology*, *23*, 2273–2278. https://doi.org/10.1016/j.cub.2013.09.020, PubMed: 24184106

Heinrich, S. P. (2010). Some thoughts on the interpretation of steady-state evoked potentials. *Documenta Ophthalmologica*, *120*, 205–214. https://doi.org/10.1007/s10633-010-9212-7, PubMed: 20101435

Henry, M. J., Herrmann, B., & Obleser, J. (2014). Entrained neural oscillations in multiple frequency bands comodulate behavior. *Proceedings of the National Academy of Sciences, U.S.A.*, *111*, 14935–14940. https://doi.org/10.1073/pnas.1408741111, PubMed: 25267634

Henry, M. J., & Obleser, J. (2012). Frequency modulation entrains slow neural oscillations and optimizes human listening behavior. *Proceedings of the National Academy of Sciences, U.S.A.*, *109*, 20095–20100. https://doi.org/10.1073/pnas.1213390109, PubMed: 23151506

Horton, J. C., & Hoyt, W. F. (1991). The representation of the visual field in human striate cortex: A revision of the classic Holmes map. *Archives of Ophthalmology*, *109*, 816–824. https://doi.org/10.1001/archopht.1991.01080060080030, PubMed: 2043069

Huang, Y., Chen, L., & Luo, H. (2015). Behavioral oscillation in priming: Competing perceptual predictions conveyed in alternating theta-band rhythms. *Journal of Neuroscience*, *35*, 2830–2837. https://doi.org/10.1523/JNEUROSCI.4294-14.2015, PubMed: 25673869

Huang, X., Troy, W. C., Yang, Q., Ma, H., Laing, C. R., Schiff, S. J., et al. (2004). Spiral waves in disinhibited mammalian neocortex. *Journal of Neuroscience*, *24*, 9897–9902. https://doi.org/10.1523/JNEUROSCI.2705-04.2004, PubMed: 15525774

Jancke, D., Chavane, F., Naaman, S., & Grinvald, A. (2004). Imaging cortical correlates of illusion in early visual cortex. *Nature*, *428*, 423–426. https://doi.org/10.1038/nature02396, PubMed: 15042090

Keitel, C., Ruzzoli, M., Dugué, L., Busch, N. A., & Benwell, C. S. Y. (2022). Rhythms in cognition: The evidence revisited. *European Journal of Neuroscience*, *55*, 2991–3009. https://doi.org/10.1111/ejn.15740, PubMed: 35696729

Kienitz, R., Schmid, M. C., & Dugué, L. (2022). Rhythmic sampling revisited: Experimental paradigms and neural mechanisms. *European Journal of Neuroscience*, *55*, 3010–3024. https://doi.org/10.1111/ejn.15489, PubMed: 34643973

Kizuk, S. A. D., & Mathewson, K. E. (2017). Power and phase of alpha oscillations reveal an interaction between spatial and temporal visual attention. *Journal of Cognitive Neuroscience*, *29*, 480–494. https://doi.org/10.1162/jocn_a_01058, PubMed: 28129063

Landau, A. N., & Fries, P. (2012). Attention samples stimuli rhythmically. *Current Biology*, 22, 1000–1004. https://doi.org/10.1016/j.cub.2012.03.054, PubMed: 22633805

Lippert, M. T., Takagaki, K., Xu, W., Huang, X., & Wu, J.-Y. (2007). Methods for voltage-sensitive dye imaging of rat cortical activity with high signal-to-noise ratio. *Journal of Neurophysiology*, 98, 502–512. https://doi.org/10.1152/jn.01169.2006, PubMed: 17493915

Liu-Shuang, J., Norcia, A. M., & Rossion, B. (2014). An objective index of individual face discrimination in the right occipito-temporal cortex by means of fast periodic oddball stimulation. *Neuropsychologia*, 52, 57–72. https://doi.org/10.1016/j.neuropsychologia.2013.10.022, PubMed: 24200921

Maris, E., Womelsdorf, T., Desimone, R., & Fries, P. (2013). Rhythmic neuronal synchronization in visual cortex entails spatial phase relation diversity that is modulated by stimulation and attention. *Neuroimage*, 74, 99–116. https://doi.org/10.1016/j.neuroimage.2013.02.007, PubMed: 23416733

Mathewson, K. E., Gratton, G., Fabiani, M., Beck, D. M., & Ro, T. (2009). To see or not to see: Prestimulus α phase predicts visual awareness. *Journal of Neuroscience*, 29, 2725–2732. https://doi.org/10.1523/JNEUROSCI.3963-08.2009, PubMed: 19261866

Mathewson, K. E., Prudhomme, C., Fabiani, M., Beck, D. M., Lleras, A., & Gratton, G. (2012). Making waves in the stream of consciousness: Entraining oscillations in EEG alpha and fluctuations in visual awareness with rhythmic visual stimulation. *Journal of Cognitive Neuroscience*, 24, 2321–2333. https://doi.org/10.1162/jocn_a_00288, PubMed: 22905825

Merholz, G., Grabot, L., VanRullen, R., & Dugué, L. (2022). Periodic attention operates faster during more complex visual search. *Scientific Reports*, 12, 6688. https://doi.org/10.1038/s41598-022-10647-5, PubMed: 35461325

Michel, R., Dugué, L., & Busch, N. A. (2022). Distinct contributions of alpha and theta rhythms to perceptual and attentional sampling. *European Journal of Neuroscience*, 55, 3025–3039. https://doi.org/10.1111/ejn.15154, PubMed: 33609313

Muller, L., Chavane, F., Reynolds, J., & Sejnowski, T. J. (2018). Cortical travelling waves: Mechanisms and computational principles. *Nature Reviews Neuroscience*, 19, 255–268. https://doi.org/10.1038/nrn.2018.20, PubMed: 29563572

Muller, L., Reynaud, A., Chavane, F., & Destexhe, A. (2014). The stimulus-evoked population response in visual cortex of awake monkey is a propagating wave. *Nature Communications*, 5, Article 3675. https://doi.org/10.1038/ncomms4675, PubMed: 24770473

Nauhaus, I., Busse, L., Carandini, M., & Ringach, D. L. (2009). Stimulus contrast modulates functional connectivity in visual cortex. *Nature Neuroscience*, 12, 70–76. https://doi.org/10.1038/nn.2232, PubMed: 19029885

Nauhaus, I., Busse, L., Ringach, D. L., & Carandini, M. (2012). Robustness of traveling waves in ongoing activity of visual cortex. *Journal of Neuroscience*, 32, 3088–3094. https://doi.org/10.1523/JNEUROSCI.5827-11.2012, PubMed: 22378881

Norcia, A. M., Appelbaum, L. G., Ales, J. M., Cottereau, B. R., & Rossion, B. (2015). The steady-state visual evoked potential in vision research: A review. *Journal of Vision*, 15, 4. https://doi.org/10.1167/15.6.4, PubMed: 26024451

Nowak, L. G., & Bullier, J. (1996). Spread of stimulating current in the cortical grey matter of rat visual cortex studied on a new in vitro slice preparation. *Journal of Neuroscience Methods*, 67, 237–248. https://doi.org/10.1016/0165-0270(96)00065-9, PubMed: 8872891

Prechtl, J. C., Bullock, T. H., & Kleinfeld, D. (2000). Direct evidence for local oscillatory current sources and intracortical phase gradients in turtle visual cortex. *Proceedings of the National Academy of Sciences, U.S.A.*, 97, 877–882. https://doi.org/10.1073/pnas.97.2.877, PubMed: 10639173

Prechtl, J. C., Cohen, L. B., Pesaran, B., Mitra, P. P., & Kleinfeld, D. (1997). Visual stimuli induce waves of electrical activity in turtle cortex. *Proceedings of the National Academy of Sciences, U.S.A.*, 94, 7621–7626. https://doi.org/10.1073/pnas.94.14.7621, PubMed: 9207142

Purves, D., Paydarfar, J. A., & Andrews, T. J. (1996). The wagon wheel illusion in movies and reality. *Proceedings of the National Academy of Sciences, U.S.A.*, 93, 3693–3697. https://doi.org/10.1073/pnas.93.8.3693, PubMed: 8622999

Ray, S., & Maunsell, J. H. R. (2011). Different origins of gamma rhythm and high-gamma activity in macaque visual cortex. *PLoS Biology*, 9, e1000610. https://doi.org/10.1371/journal.pbio.1000610, PubMed: 21532743

Re, D., Karvat, G., & Landau, A. N. (2023). Attentional sampling between eye channels. *Journal of Cognitive Neuroscience*, 35, 1350–1360. https://doi.org/10.1162/jocn_a_02018, PubMed: 37315334

Reed, A. V. (1973). Speed–accuracy trade-off in recognition memory. *Science*, 181, 574–576. https://doi.org/10.1126/science.181.4099.574, PubMed: 17777808

Rekauzke, S., Nortmann, N., Staadt, R., Hock, H. S., Schöner, G., & Jancke, D. (2016). Temporal asymmetry in dark–bright processing initiates propagating activity across primary visual cortex. *Journal of Neuroscience*, 36, 1902–1913. https://doi.org/10.1523/JNEUROSCI.3235-15.2016, PubMed: 26865614

Reynaud, A., Masson, G. S., & Chavane, F. (2012). Dynamics of local input normalization result from balanced short- and long-range intracortical interactions in area V1. *Journal of Neuroscience*, 32, 12558–12569. https://doi.org/10.1523/JNEUROSCI.1618-12.2012, PubMed: 22956845

Roland, P. E., Hanazawa, A., Undeman, C., Eriksson, D., Tompa, T., Nakamura, H., et al. (2006). Cortical feedback depolarization waves: A mechanism of top–down influence on early visual areas. *Proceedings of the National Academy of Sciences, U.S.A.*, 103, 12586–12591. https://doi.org/10.1073/pnas.0604925103, PubMed: 16891418

Rossion, B., Prieto, E. A., Boremanse, A., Kuefner, D., & Van Belle, G. (2012). A steady-state visual evoked potential approach to individual face perception: Effect of inversion, contrast-reversal and temporal dynamics. *Neuroimage*, 63, 1585–1600. https://doi.org/10.1016/j.neuroimage.2012.08.033, PubMed: 22917988

Rubino, D., Robbins, K. A., & Hatsopoulos, N. G. (2006). Propagating waves mediate information transfer in the motor cortex. *Nature Neuroscience*, 9, 1549–1557. https://doi.org/10.1038/nn1802, PubMed: 17115042

Samaha, J., Gosseries, O., & Postle, B. R. (2017). Distinct oscillatory frequencies underlie excitability of human occipital and parietal cortex. *Journal of Neuroscience*, 37, 2824–2833. https://doi.org/10.1523/JNEUROSCI.3413-16.2017, PubMed: 28179556

Samaha, J., & Postle, B. R. (2015). The speed of alpha-band oscillations predicts the temporal resolution of visual perception. *Current Biology*, 25, 2985–2990. https://doi.org/10.1016/j.cub.2015.10.007, PubMed: 26526370

Sanchez-Vives, M. V., & McCormick, D. A. (2000). Cellular and network mechanisms of rhythmic recurrent activity in neocortex. *Nature Neuroscience*, 3, 1027–1034. https://doi.org/10.1038/79848, PubMed: 11017176

Sato, T. K., Nauhaus, I., & Carandini, M. (2012). Traveling waves in visual cortex. *Neuron*, 75, 218–229. https://doi.org/10.1016/j.neuron.2012.06.029, PubMed: 22841308

Senoussi, M., Moreland, J. C., Busch, N. A., & Dugué, L. (2019). Attention explores space periodically at the theta frequency. *Journal of Vision*, 19, 22. https://doi.org/10.1167/19.5.22, PubMed: 31121012

Shao, Z., & Burkhalter, A. (1996). Different balance of excitation and inhibition in forward and feedback circuits of rat visual

cortex. *Journal of Neuroscience, 16*, 7353–7365. https://doi
.org/10.1523/JNEUROSCI.16-22-07353.1996, PubMed: 8929442

Sharon, D., Jancke, D., Chavane, F., Na'aman, S., & Grinvald, A.
(2007). Cortical response field dynamics in cat visual cortex.
Cerebral Cortex, 17, 2866–2877. https://doi.org/10.1093
/cercor/bhm019, PubMed: 17395608

Sit, Y. F., Chen, Y., Geisler, W. S., Miikkulainen, R., &
Seidemann, E. (2009). Complex dynamics of V1 population
responses explained by a simple gain-control model. *Neuron,
64*, 943–956. https://doi.org/10.1016/j.neuron.2009.08.041,
PubMed: 20064399

Slovin, H., Arieli, A., Hildesheim, R., & Grinvald, A. (2002).
Long-term voltage-sensitive dye imaging reveals cortical
dynamics in behaving monkeys. *Journal of Neurophysiology,
88*, 3421–3438. https://doi.org/10.1152/jn.00194.2002,
PubMed: 12466458

Sokoliuk, R., & VanRullen, R. (2016). Global and local oscillatory
entrainment of visual behavior across retinotopic space.
Scientific Reports, 6, 25132. https://doi.org/10.1038
/srep25132, PubMed: 27126642

Song, K., Meng, M., Chen, L., Zhou, K., & Luo, H. (2014).
Behavioral oscillations in attention: Rhythmic α pulses
mediated through θ band. *Journal of Neuroscience, 34*,
4837–4844. https://doi.org/10.1523/JNEUROSCI.4856-13
.2014, PubMed: 24695703

Spaak, E., de Lange, F. P., & Jensen, O. (2014). Local
entrainment of α oscillations by visual stimuli causes cyclic
modulation of perception. *Journal of Neuroscience, 34*,
3536–3544. https://doi.org/10.1523/JNEUROSCI.4385-13
.2014, PubMed: 24599454

Sreekumar, V., Wittig, J. H., Jr., Chapeton, J. I., Inati, S. K., &
Zaghloul, K. A. (2020). Low frequency traveling waves in the
human cortex coordinate neural activity across spatial scales.
BioRxiv, 2020-03, 1–48. https://doi.org/10.1101/2020.03.04
.977173

Stefanics, G., Hangya, B., Hernádi, I., Winkler, I., Lakatos, P., &
Ulbert, I. (2010). Phase entrainment of human delta oscillations
can mediate the effects of expectation on reaction speed.
Journal of Neuroscience, 30, 13578–13585. https://doi.org/10
.1523/JNEUROSCI.0703-10.2010, PubMed: 20943899

Stroh, A., Adelsberger, H., Groh, A., Rühlmann, C., Fischer, S.,
Schierloh, A., et al. (2013). Making waves: Initiation and
propagation of corticothalamic Ca2+ waves in vivo. *Neuron,
77*, 1136–1150. https://doi.org/10.1016/j.neuron.2013.01.031,
PubMed: 23522048

Takagaki, K., Zhang, C., Wu, J.-Y., & Lippert, M. T. (2008).
Crossmodal propagation of sensory-evoked and spontaneous
activity in the rat neocortex. *Neuroscience Letters, 431*,
191–196. https://doi.org/10.1016/j.neulet.2007.11.069,
PubMed: 18178313

Takahashi, K., Kim, S., Coleman, T. P., Brown, K. A., Suminski,
A. J., Best, M. D., et al. (2015). Large-scale spatiotemporal
spike patterning consistent with wave propagation in motor
cortex. *Nature Communications, 6*, 7169. https://doi.org/10
.1038/ncomms8169, PubMed: 25994554

Takahashi, K., Saleh, M., Penn, R. D., & Hatsopoulos, N. G.
(2011). Propagating waves in human motor cortex. *Frontiers
in Human Neuroscience, 5*, 40. https://doi.org/10.3389
/fnhum.2011.00040, PubMed: 21629859

Ten Oever, S., & Sack, A. T. (2015). Oscillatory phase shapes
syllable perception. *Proceedings of the National Academy of
Sciences, U.S.A., 112*, 15833–15837. https://doi.org/10.1073
/pnas.1517519112, PubMed: 26668393

Townsend, R. G., Solomon, S. S., Chen, S. C., Pietersen, A. N. J.,
Martin, P. R., Solomon, S. G., et al. (2015). Emergence of
complex wave patterns in primate cerebral cortex. *Journal of
Neuroscience, 35*, 4657–4662. https://doi.org/10.1523
/JNEUROSCI.4509-14.2015, PubMed: 25788682

Valera, F. J., Toro, A., John, E. R., & Schwartz, E. L. (1981).
Perceptual framing and cortical alpha rhythm.
Neuropsychologia, 19, 675–686. https://doi.org/10.1016/0028
-3932(81)90005-1, PubMed: 7312152

VanRullen, R. (2007). The continuous wagon wheel illusion
depends on, but is not identical to neuronal adaptation.
Vision Research, 47, 2143–2149. https://doi.org/10.1016/j
.visres.2007.03.019, PubMed: 17559904

VanRullen, R. (2016). Perceptual cycles. *Trends in Cognitive
Sciences, 20*, 723–735. https://doi.org/10.1016/j.tics.2016.07
.006, PubMed: 27567317

VanRullen, R., & Dubois, J. (2011). The psychophysics of brain
rhythms. *Frontiers in Psychology, 2*, 203. https://doi.org/10
.3389/fpsyg.2011.00203, PubMed: 21904532

VanRullen, R., & Koch, C. (2003). Is perception discrete or
continuous? *Trends in Cognitive Sciences, 7*, 207–213. https://
doi.org/10.1016/S1364-6613(03)00095-0, PubMed: 12757822

VanRullen, R., Reddy, L., & Koch, C. (2005). Attention-driven
discrete sampling of motion perception. *Proceedings of the
National Academy of Sciences, U.S.A., 102*, 5291–5296.
https://doi.org/10.1073/pnas.0409172102, PubMed: 15793010

VanRullen, R., Reddy, L., & Koch, C. (2006). The continuous
wagon wheel illusion is associated with changes in
electroencephalogram power at ~13 Hz. *Journal of
Neuroscience, 26*, 502–507. https://doi.org/10.1523
/JNEUROSCI.4654-05.2006, PubMed: 16407547

Wandell, B. A., & Winawer, J. (2011). Imaging retinotopic maps
in the human brain. *Vision Research, 51*, 718–737. https://doi
.org/10.1016/j.visres.2010.08.004, PubMed: 20692278

Watt, J., Borhani, R., & Katsaggelos, A. K. (2020). *Machine
learning refined: Foundations, algorithms, and
applications*. Cambridge, UK: Cambridge University Press.
https://doi.org/10.1017/9781108690935

Wickelgren, W. A. (1977). Speed–accuracy tradeoff and
information processing dynamics. *Acta Psychologica, 41*,
67–85. https://doi.org/10.1016/0001-6918(77)90012-9

Xu, W., Huang, X., Takagaki, K., & Wu, J.-Y. (2007).
Compression and reflection of visually evoked cortical waves.
Neuron, 55, 119–129. https://doi.org/10.1016/j.neuron.2007
.06.016, PubMed: 17610821

Yang, Z., Heeger, D. J., Blake, R., & Seidemann, E. (2015). Long-
range traveling waves of activity triggered by local dichoptic
stimulation in V1 of behaving monkeys. *Journal of
Neurophysiology, 113*, 277–294. https://doi.org/10.1152/jn
.00610.2013, PubMed: 25343785

Zanos, T. P., Mineault, P. J., Nasiotis, K. T., Guitton, D., & Pack,
C. C. (2015). A sensorimotor role for traveling waves in
primate visual cortex. *Neuron, 85*, 615–627. https://doi.org/10
.1016/j.neuron.2014.12.043, PubMed: 25600124

Zhang, H., & Jacobs, J. (2015). Traveling theta waves in the
human hippocampus. *Journal of Neuroscience, 35*,
12477–12487. https://doi.org/10.1523/JNEUROSCI.5102-14
.2015, PubMed: 26354915

Zhang, Q., Wen, Y., Zhang, D., She, L., Wu, J., Dan, Y., et al.
(2012). Priming with real motion biases visual cortical
response to bistable apparent motion. *Proceedings of the
National Academy of Sciences, U.S.A., 109*, 20691–20696.
https://doi.org/10.1073/pnas.1218654109, PubMed: 23188797